Remote Sensing of Environment 151 (2014) 102–113

Contents lists available at ScienceDirect

Remote Sensing of Environment

journal homepage: www.elsevier.com/locate/rse

Detecting mortality induced structural and functional changes in a piñon-juniper woodland using Landsat and RapidEye time series

Dan J. Krofcheck [a,*], Jan U.H. Eitel [b,c], Lee A. Vierling [b,c], Urs Schulthess [d], Timothy M. Hilton [a], Eva Dettweiler-Robinson [a], Rosemary Pendleton [e], Marcy E. Litvak [a]

[a] Department of Biology, University of New Mexico, Albuquerque, NM 87131, USA
[b] Geospatial Laboratory for Environmental Dynamics, University of Idaho, Moscow, ID 83844-1135, USA
[c] McCall Outdoor Science School, University of Idaho, McCall, ID 83638, USA
[d] 4DMaps, Wörther Str. 33, 10405 Berlin, Germany
[e] USDA Forest Service, Rocky Mountain Research Station, Albuquerque, NM 87102, USA

ARTICLE INFO

Article history:
Received 16 January 2013
Received in revised form 1 November 2013
Accepted 1 November 2013
Available online 25 December 2013

Keywords:
Semi-arid
High resolution
Time-series
Ecosystem disturbance
Eddy-covariance
Red-edge

ABSTRACT

Piñon–juniper (PJ) woodlands have recently undergone dramatic drought-induced mortality, triggering broad scale structural changes in this extensive Southwestern US biome. Given that climate projections for the region suggest widespread conifer mortality is likely to continue into the next century, it is critical to better understand how this climate-induced change in vegetation structure alters ecosystem function (e.g., productivity, biogeochemical cycling, energy partitioning) in PJ woodlands. Data from satellite remote sensing could potentially help to gain some of this understanding. However, relatively little is known about the suitability of satellite remote sensing for monitoring mortality induced structural and functional changes in PJ woodlands, a semi-arid biome characterized by sparse vegetation that complicates remote sensing of vegetation properties. Here we examined the potential role of satellite remote sensing to better understand structural and functional changes that take place in PJ woodlands as they respond to and recover from climate induced mortality events. We used time series medium (30 × 30 m) and high (≤5 × 5 m) spatial resolution satellite data in concert with eddy covariance-based gross primary productivity (GPP) data collected in a PJ woodland mortality manipulation near Mountainair, NM. Our results showed that both high and medium resolution satellite remote sensing data can provide ecosystem level assessments of overall canopy mortality and subsequent regrowth in these semi-arid woodlands. However, high spatial resolution data allowed detecting the disturbance almost a full year earlier and enabled us to describe the spatially heterogeneous patterns of recovery typical for such complex. The ability of satellite remote sensing to be used to provide information about changes in ecosystem function was conditional on the presence of sufficient soil moisture; when soil moisture was present the strength of the linear relationship between GPP and spectral vegetation indices improved at the manipulated site (e.g. for high resolution NDVI data $R^2 = 0.13$ during drought conditions, $R^2 = 0.46$ when wet, $P < .05$) and less so at a nearby control site ($R^2 = 0.09$ during drought conditions, compared to $R^2 = 0.22$ during growing conditions, $P < .05$). Thus, although satellite time series can be used to monitor and improve our understanding of canopy function in both disturbed and undisturbed semi-arid coniferous biomes, combining in situ eddy covariance data with satellite time series demonstrated that the utility of these datasets is highest during periods of peak growing conditions. This study therefore provides a benchmark for understanding how spatial and temporal variation in vegetation structure and function can be best studied as semi-arid coniferous biomes respond to future climate variability.

1. Introduction

Climatic conditions and disturbance events that cause tree mortality are predicted to become more severe and frequent, resulting in widespread ecological changes at scales ranging from landscapes to regions (Williams, Allen, & Macalady, 2012; Choat et al., 2012). However, the impacts of disturbance on ecological function are often poorly understood and are therefore seldom included in broad scale models of forest productivity (Liu, Bond-Lamberty, & Hicke, 2011). For example,

* Corresponding author at: University of New Mexico, Department of Biology, 1 University Boulevard Northeast, Albuquerque, NM 87131, USA. Tel.: +1 505 277 8685.
E-mail addresses: djkrofch@unm.edu (D.J. Krofcheck), jeitel@uidaho.edu (J.U.H. Eitel), leev@uidaho.edu (L.A. Vierling), uschulthess@gmail.com (U. Schulthess), evadr@unm.edu (E. Dettweiler-Robinson), rpendleton@fs.fed.us (R. Pendleton), mlitvak@unm.edu (M.E. Litvak).

0034-4257/$ – see front matter © 2013 Elsevier Inc. All rights reserved.
http://dx.doi.org/10.1016/j.rse.2013.11.009

feedbacks associated with significant increases in forest mortality across the globe have potentially caused changes in global temperature and precipitation amount and variability, particularly in the past decade (Allen et al., 2010; IPCC, 2007). Large scale vegetation mortality is likely to cause increased CO_2 flux to the atmosphere in the short term and can lead to lasting changes in ecosystem structure (e.g., reductions in canopy leaf area and changes in understory species composition) with long-term (>decadal scale) effects on ecosystem carbon and energy balance (Allen et al., 2010; Adams et al., 2010). A mechanistic understanding is necessary to further elucidate how these mortality induced structural changes relate to changes in functional processes such as energy partitioning, vegetation productivity, and carbon sequestration, and to quantify the impact of these mortality events on terrestrial productivity and/or climate at multiple spatial and temporal scales.

In the southwestern US, conditions that trigger tree mortality (e.g., low water availability and high temperature) are predicted to become more in the next century resulting in increasing tree mortality (Williams et al., 2012). Widespread tree mortality quickly alters the physical structure of the ecosystem in terms of both the rapid changes to the woody overstory and the subsequent responses of the understory vegetation caused by changes in light, moisture, and nutrient availability (Rich, Breshears, & White, 2008). One biome that appears to be very sensitive to climate variability in the southwestern US is piñon-pine/juniper (PJ) woodland, which covers over 24 million ha in the region (Fig. 1). A severe drought in New Mexico, Colorado, Utah and Arizona from 1999 to 2002 (Breshears et al., 2005; Schwalm et al., 2012; Williams et al., 2012) caused dramatic structural change to over 1.5million ha of PJ woodlands due to the abrupt die-off of 40–95% piñon-pine (*Pinus edulis*) and 2–25% one-seed juniper (*Juniperous monosperma*) (Breshears et al., 2005; Shaw, Steed, & DeBlander, 2005; Williams et al., 2010). The resulting differential mortality of the overstory in PJ woodlands has had severe and lasting effects on ecosystem structure. Needle fall from the dead piñon began 6–12 months following mortality (Royer et al., 2011), and the biomass of herbaceous understory increased in response to higher light and soil moisture availability (Rich et al., 2008). Following mortality, stand age structure in these biomes shifted towards a mixture of juniper and juvenile (non-reproductive) piñon, lowering the average canopy height and average stem diameter of the system (Clifford, Rocca, & Delph, 2008). These structural changes may create legacies of functional change with unknown implications for the carbon, water and energy balance of these disturbed woodlands. Given the broad spatial extent of PJ woodlands across the US, coupled with this biome's high sensitivity to climate change induced drought, it is imperative that methods are developed to understand how structural changes in PJ woodlands following mortality events affect the carbon and water balance of this biome.

Much research has focused on the use of satellite remote sensing to monitor and quantify changes in forest structure following disturbances such as insect outbreaks and severe drought (e.g., Coops et al., 2006, Huang, Asner, & Barger, 2012; Huang, Asner, Barger, Neff, & Floyd, 2010; Kennedy, Cohen, & Schroeder, 2007; Spruce, Sader, Ryan, & Smoot, 2010; Wulder et al., 2006). The majority of this work has examined forest ecosystems characterized by dense vegetation (LAI > 1.5). However, semi-arid biomes are characterized by sparse vegetation (LAI < 1.5) which poses unique challenges to using a multi-temporal approach that detects structural change as anomalous deviations from long-term or short-term seasonal trends (e.g., Huang et al., 2010; Kennedy, Yang, & Cohen, 2010). In ecosystems with sparse vegetation, the measured spectral radiance is strongly influenced by the soil background, which confounds the vegetation spectral signal and thus the ability to remotely sense structural changes over time (e.g., Eitel, Long, Gessler, Hunt, & Brown, 2009; Huete et al., 1985, 1988).

To reduce the confounding effects of soil background on remote sensing of vegetation, spectral mixture analysis (SMA) may be used to isolate the vegetation spectral signal from the spectral signal obtained from the soil (Asner and Heidebrecht, 2002; Elmore et al., 2000;

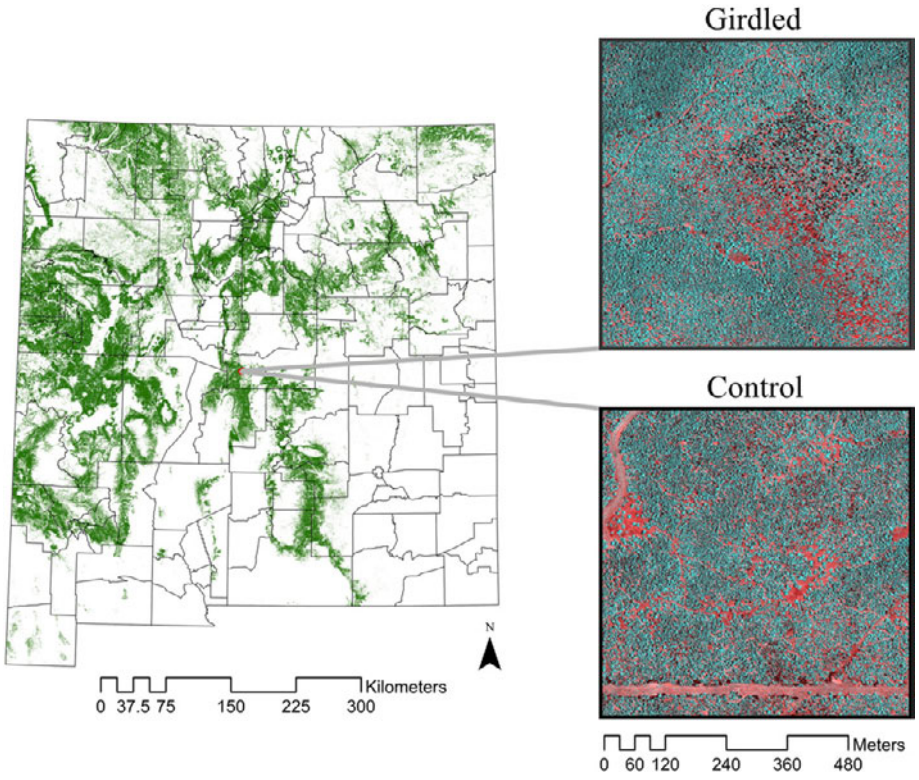

Fig. 1. The study sites are located <3 km apart from each other in central New Mexico. The extent of Piñon–juniper woodland across the state is shown in green.

Huang et al., 2010; Li, Gao, Bai, & Huang, 2012). By decomposing a satellite pixel into its components, SMA can provide the fractional cover of both photosynthetic and non-photosynthetic vegetation, as well as the fraction of bare soil and shadow. For example, Huang et al. (2010) leveraged the spectral resolution of Landsat TM and ETM+ data to characterize the fractional cover of woody and herbaceous vegetation in a semi-arid woodland. However, in order to describe sub-pixel cover SMA relies on either spectral libraries or ground collected spectra, both of which rely on data that can be sensitive to temporal and spatial variability of vegetation, rock and soil, as well as the scale at which the spectra were collected (Asner and Heidebrecht, 2002).

The challenge of characterizing sparse vegetation in semi-arid systems may be partially overcome by using high ($\leq 5 \times 5$ m) spatial resolution satellite data. This scale of data is helpful in sparsely wooded areas in particular, because it often allows individual tree crowns to be resolved for analysis (Chen et al., 2004; Storey, 2004; Tong & He, 2013). However, relatively little is known about the use of high spatial resolution satellite imagery to monitor and quantify structural changes in semi-arid biomes following disturbance events. Even if high spatial resolution imagery may allow improved monitoring of structural changes in semi-arid ecosystems, relatively little is known about how these structural changes can be linked to changes in ecosystem function, namely changes in gross primary production (GPP).

Our overall objective was to examine the potential role of satellite remote sensing towards an improved understanding of mortality induced structural and functional changes in a PJ woodland. Specifically, we tested i) the suitability of satellite time series for monitoring mortality induced structural changes and subsequent changes in ecosystem function in PJ woodlands and ii) how the suitability of satellite remote sensing for monitoring these structural and functional changes is affected by the spatial resolution of the employed satellite imagery. To investigate these questions we used time series of medium (30 × 30 m; Landsat ETM+) and high spatial resolution (5 × 5 m; RapidEye) satellite data in concert with GPP data collected in a PJ woodland mortality manipulation experiment near Mountainair, NM.

2. Methods

2.1. Site description

The study area includes two piñon–juniper woodlands separated by 3 km and located south of Mountainair, NM (Fig. 1). In September of 2009, 1632 adult piñon (>7 cm diameter at breast height) in a 4 ha plot in one of the sites (hereafter referred to as the girdled site; 34° 26′ 48.54″ N, 106° 12′ 48.63″ W) were mechanically girdled by severing the sapwood with a chainsaw at breast height (1.4 m) followed by the application of a 5% glyphosate solution directly applied to the cut to ensure rapid loss of conductivity and subsequent mortality of the trees. The total decoupling of the leaves with the roots following the manipulation was designed to replicate the landscape following the mortality that occurred in the response to the 1999–2002 drought (Breshears et al., 2005; Clifford et al., 2008). The second PJ woodland (hereafter referred to as the control site; 34° 26′ 18.420″ N, 106° 14′ 15.698″ W) remained intact. We have continually monitored surface fluxes of carbon, water and energy at each site using tower mounted eddy covariance and associated micrometeorological sensors since 8 months prior to the girdling manipulation in February 2009 (Fox et al., 2013).

The soil at both sites is Turkey Springs stony loam, characterized by an abundance of alluvially deposited limestone (Soil Survey Staff). The climate of the region is semi-arid, with a mean annual precipitation of 372 mm (±86.8 mm standard deviation, sd) and mean, max, and min temperatures of 19.8 °C (±0.77 °C sd) and 2.32 °C (±0.64 °C sd) respectively, over the past 20 years (PRISM Climate Group, Oregon State University, http://prism.oregonstate.edu, created 28 June 2004). Incoming moisture to the site is largely bimodal, broken into winter snow melt from January to March and seasonal monsoon precipitation between August and October with a pronounced dry season occurring from April through July.

2.2. In situ field measurements

Eddy covariance derived surface fluxes of carbon dioxide, water and energy were measured at 10 Hz using a 3-axis sonic anemometer (CSAT-3, Campbell Scientific, Logan, UT, USA) and an open path infrared gas analyzer (Li-7500, LiCor Biosciences; Lincoln, NE, USA).

Continuous measures of net radiation, air temperature and relative humidity, soil temperature, photosynthetically active radiation, and soil moisture were made using a CNR1 (Kipp and Zonen, Delft, Netherlands), HMP45C (Vaisala RH probe with aspirated radiation shield Helsinki, Finland), TCAV (averaging thermocouple probes, 27 per site), and up-facing quantum sensors (Li-190SB, Licor Biosciences) respectively. ECHO probes (TE 5 cm, Decagon Devices, Pullman, WA, 27 per site) were used for the measurements of volumetric water content (VWC) at each site. The fluxes were aggregated to 30 min intervals and were corrected for temperature and moisture variations (WPL, Webb, Pearman, & Leuning, 1980) as well as frequency responses according to Massman (2000) as described in Anderson-Teixera et al. (2011). Anemometer tilt due to terrain variability was corrected using a planar fit method. We used a friction velocity (u*) filter to reject data obtained when turbulence was low (u* less than a threshold value). Data gaps created by the u* filter, malfunctioning instruments, and rain were filled following Lasslop et al. (2010). We partitioned the gapfilled net ecosystem exchange (NEE) into the components of total C uptake through photosynthesis or Gross Primary Productivity (GPP), and total carbon leaving the ecosystem through both autotrophic and heterotrophic respiration (Re). We used exponential relationships between nighttime NEE and temperature following the methods of Lasslop et al. (2010) to calculate continuous ecosystem respiration during the day. GPP was then calculated as NEE − Re (Flanagan, Wever, & Carlson, 2002).

2.3. Plot level vegetation sampling

In 2008 (before the girdling treatment occurred), the density of annual forbs was recorded in 1 m^2 quadrats beneath the canopy and in adjacent interspaces (outside the drip line of any trees) of seven piñon trees at each site. In 2011, four tree and interspace 0.25 m^2 quadrats at each site were monitored and permanently marked, and in 2012, those plus an additional five sets were monitored. No density monitoring occurred in 2009 or 2010. Density records for 2011 and 2012 were compared to 2008 data. A generalized linear model using backwards stepwise removal was fit to predict forb density with site, canopy vs. interspace, and the interaction term as predictor variables. Generalized linear models were fit for each year separately. All statistical analyses were run in the open-source statistical software package R 2.14.0 (R Core Team, 2012).

2.4. Remote sensing image data and pre-processing

We utilized RapidEye imagery and Landsat 7 ETM+ imagery in this study. Time series of 28 RapidEye images (September 2009 to October 2011) and 37 Landsat image dates (January 2009 to December 2012) were obtained to coincide with the girdling experiment. While we radiometrically and geometrically processed the RapidEye data in house, Landsat data were utilized as standardized downloaded products.

We obtained RapidEye data (RapidEye AG, Brandenburg, Germany) with top of atmosphere and dark object subtraction (TOA–DOS) having been performed by the vendor following standard procedures (after Collette et al., 1997; Chavez, 1988). The imagery has an orthorectified pixel size of 5 × 5 m with 5 spectral bands: blue (440–510 nm), green (520–590 nm), red (630–685 nm), red-edge (690–730 nm), and near-infrared (760–850 nm). We manually georectified each RapidEye image

to a master using 50 ground control points per image and second order polynomial transformation and nearest neighbor resampling (RMSE < 0.5 pixels). Then, we radiometrically normalized the RapidEye images using the iterative re-weighted multivariate alteration detection (IR-MAD) algorithm in Python (PythonXY ver. 2.7.3.1) (Canty & Nielsen, 2008; Nielsen, Conradsen, & Simpson, 1998).

Landsat products were downloaded in standard form for use in this study. Normalized Difference Vegetation Index (NDVI) collected by Landsat ETM+ was downloaded using the Web Enabled Landsat Database (WELD; http://globalmonitoring.sdstate.edu/projects/weld/WELD_ATBD.pdf) (Royer et al., 2011).

Vegetation indices were calculated for both regions measured by the flux towers, both as sitewide area averages (~200 × 200 m flux footprints) for Landsat and RapidEye (36 pixels for Landsat, and 1500 pixels for RapidEye) and at the single pixel scale for RapidEye for cover type averages (35 pixels per cover type). At the pixel scale, we used a cover-specific normalized difference between the two sites:

$$VI_n = (C\text{-}G)/(C + G) \quad (1)$$

where VI_n is the normalized vegetation index (VI), C is the VI value at the control site, and G is the VI value at the girdle site. The resulting VI_n values ranged between −1 and 1. This normalization allowed removal of dynamic patterns in VI that were not caused by the treatment but rather by phenology and soil moisture effects present at both sites (e.g., Eitel et al., 2011).

2.5. Pixel extraction

The extent of the tower fetch was described using a flux source area model (Hsieh, Katul, & Chi, 2000) that we expanded to two dimensions following Detto, Montaldo, Albertson, Mancini, and Katul (2006). After calculating the footprint using long-term averages of the model inputs, we georectified the model output with an image from the RapidEye derived time series and defined the tower fetch as all of the pixels falling within the 70th percentile isopleths.

To increase the signal of vegetation dynamics in this sparsely vegetated system, RapidEye pixel selection was split into two categories:

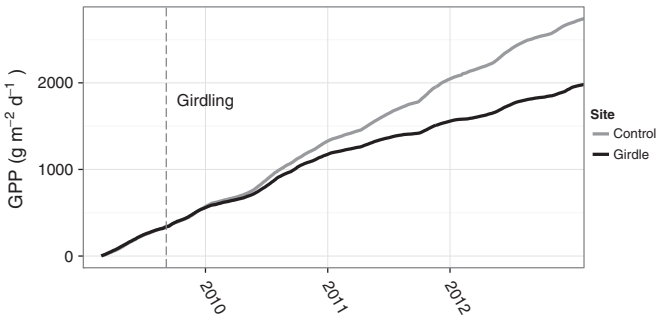

Fig. 3. Cumulative gross primary productivity throughout the manipulation for both the control (gray) and girdle (black) sites. The time of the girdling is marked with a vertical dashed line.

canopy and interspace. Canopy pixels selected for analysis in the girdled site were dominated by girdled piñon and were chosen using a multitemporal Normalized Difference Vegetation Index (NDVI) differencing technique. Images of the girdled site prior to the manipulation were subtracted from images later in the time series, in winter, fall and spring. The resulting difference images across all three seasons were used to identify change that only occurred within the tower fetch and that occurred in all three image pairs to account for seasonal green-up of herbaceous species. An equal number of pixels representing healthy canopy was selected from the control tower fetch using winter NDVI images. Interspace pixels were chosen in an identical manner but representing areas between crowns. Pixel selections at the both the girdle and control site were validated by using very high resolution (0.5 m panchromatic, 2 m multispectral), co-registered WorldView-2 (DigitalGlobe, Inc., Longmont, CO) derived site maps. We also applied this differencing technique to estimate the percent change in the fractional cover of the woody overstory that occurred at the girdle site following the manipulation, using a NDVI threshold to count pixels that had been defoliated as a result of the treatment.

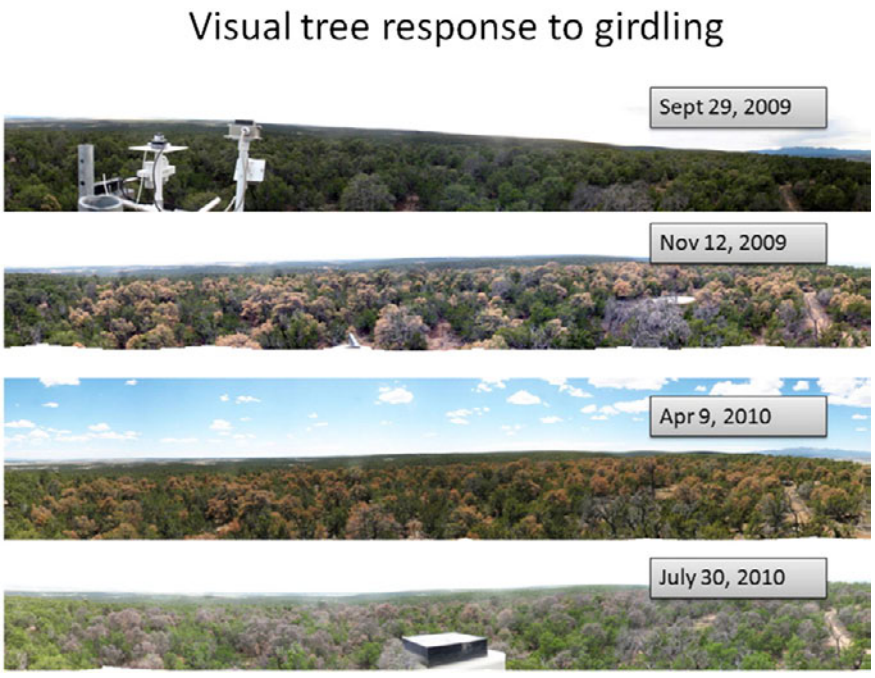

Fig. 2. A phenocam placed atop the flux tower at the girdle manipulation site provides a timeline of major, visible structural changes that took place following the manipulation, from before the manipulation took place (top) to total loss of needles on all manipulated trees (bottom).

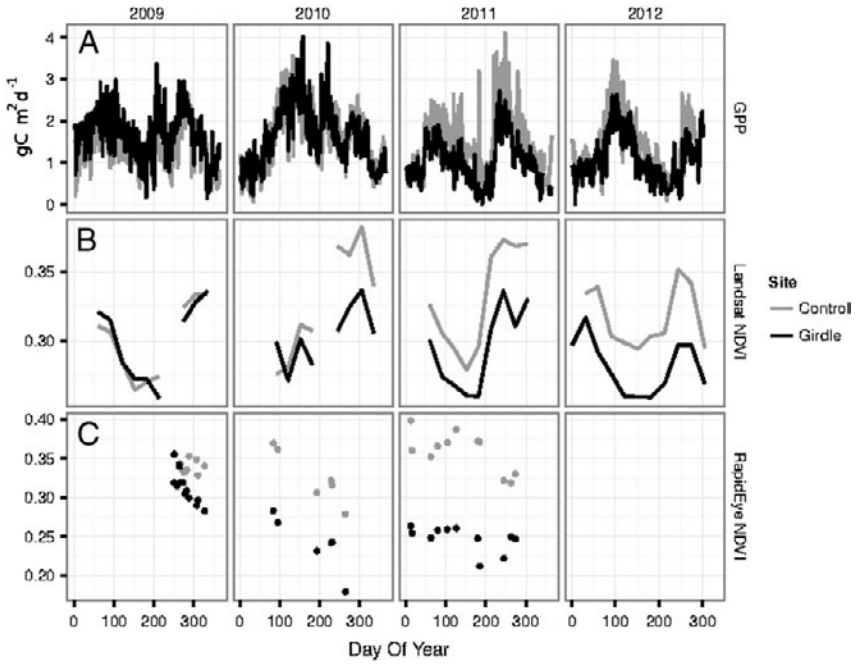

Fig. 4. Time series of A) gross primary productivity measured at the flux tower, B) Landsat ETM + derived NDVI, and C) RapidEye NDVI, for both the control (gray) and girdle (black) sites.

2.6. Vegetation index selection

Using the RapidEye dataset, we calculated three vegetation indices for our analysis: NDVI, the Normalized Difference Red Edge index (NDRE), and the Modified Soil Adjusted Vegetation Index (MSAVI2). The NDVI (Tucker, 1979) calculated as follows,

$$\mathrm{NDVI} = (\mathrm{NIR\text{-}RED}/\mathrm{NIR} + \mathrm{RED}) \quad (2)$$

where NIR is the near-infrared reflectance and RED is the red reflectance. NDVI was used because it is one of the most widely used vegetation index to probe vegetation structure (e.g., LAI) and production (e.g., GPP) (Wang et al., 2005) as well as its sensitivity in sparsely vegetated regions (Yang et al., 2012). Due to the sensitivity of NDVI to soil reflectance in low LAI systems (e.g., Huete 1989) such as PJ woodlands, and given the rapidly changing quality of the soil reflectance as a function of precipitation, we also used a second structural index MSAVI2

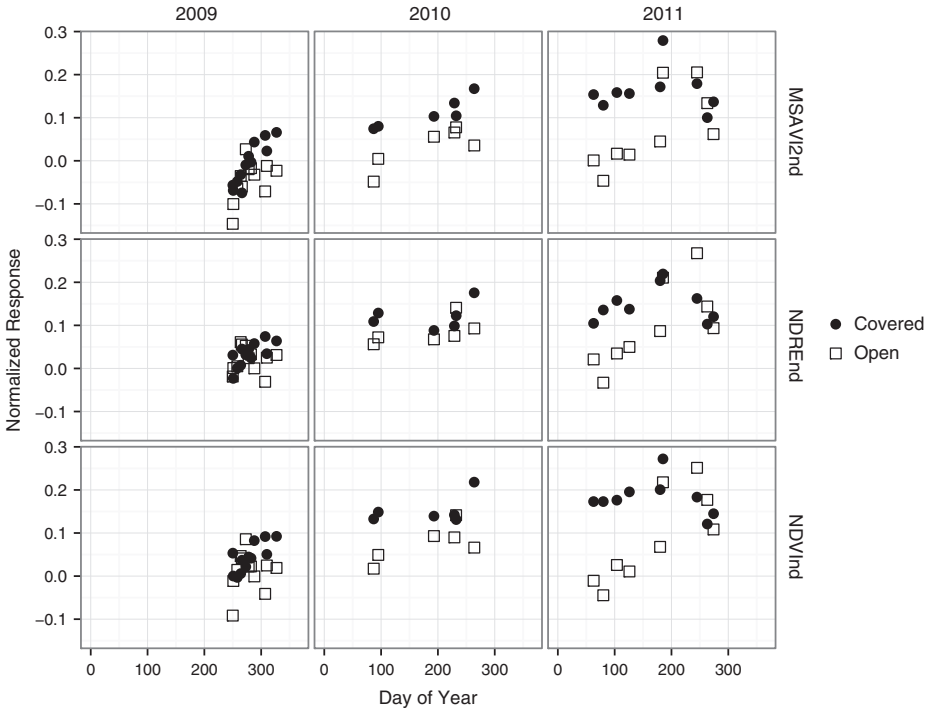

Fig. 5. RapidEye derived cover specific responses for the girdled trees (closed circles) and the spaces between girdled trees (open circles). The data are normalized relative to the control site: positive values indicate the index is greater at control.

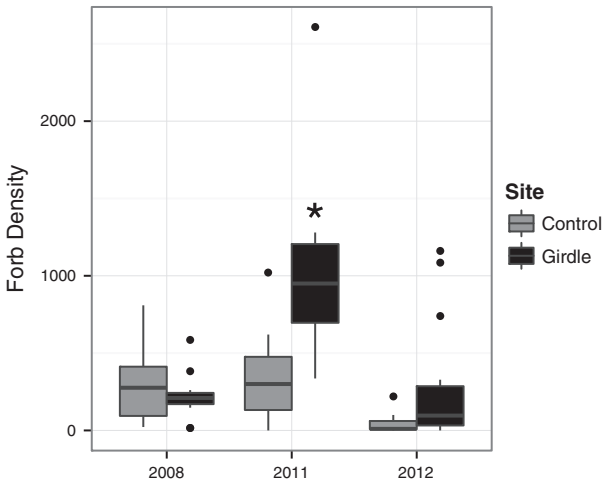

Fig. 6. Forb density before and following the manipulation at both the control (gray) and girdle (black) sites. Outliers are plotted as points, and are defined as values which are 1.5 times greater than the 75th percentile. Significance ($P < 0.001$) is marked by an asterisk.

which is designed to maximize the vegetation signal of systems with low vegetation cover and high, dynamic soil reflectance (Qi, Chehbouni, & Huete, 1994). The MSAVI2 was calculated as follows:

$$\text{MSAVI2} = \frac{2 * \text{NIR} + 1 - \sqrt{(2 * \text{NIR} + 1)^2 - 8(\text{NIR-RED})}}{2} \quad (3)$$

Finally, the NDRE was selected because of its sensitivity to both canopy structure and foliar chlorophyll concentration (Eitel et al., 2011; Gitelson & Merzlyak, 1996; Gitelson, Vina, Ciganda, & Rundquist, 2005). The latter might provide additional information when trying to link remotely sensed information to changes in plant function. The NDRE was calculated as follows:

$$\text{NDRE} = (\text{NIR-RED EDGE}/\text{NIR} + \text{RED EDGE}) \quad (4)$$

where RED EDGE is the reflectance measured in the red-edge region (690–730 nm) of the electromagnetic spectrum. NDVI products for both sites were also collected using Landsat ETM+ as described above.

3. Results

3.1. Overstory vegetation structure changes and ecosystem productivity

The selective mortality of the adult piñon in the girdled fetch took place in September of 2009. The canopy quickly became chlorotic, with large decreases in canopy chlorophyll within 22 days following the manipulation (see Eitel et al., 2011). By August 2010 all of the needles from the girdled trees had fallen to the ground (Fig. 2). Using ground based measurements and using the allometric relationship in Jenkins, Chojnacky, Heath, and Birdsey (2003), we estimated that approximately 216.5 g C m^{-2} was added to the surface as litter, which decreased LAI by 0.7 m^2 m^{-2} or roughly 33%. We validated this estimate from the allometric relationship by comparing the results to the total needle biomass measured from five trees destructively harvested from our site in 2009.

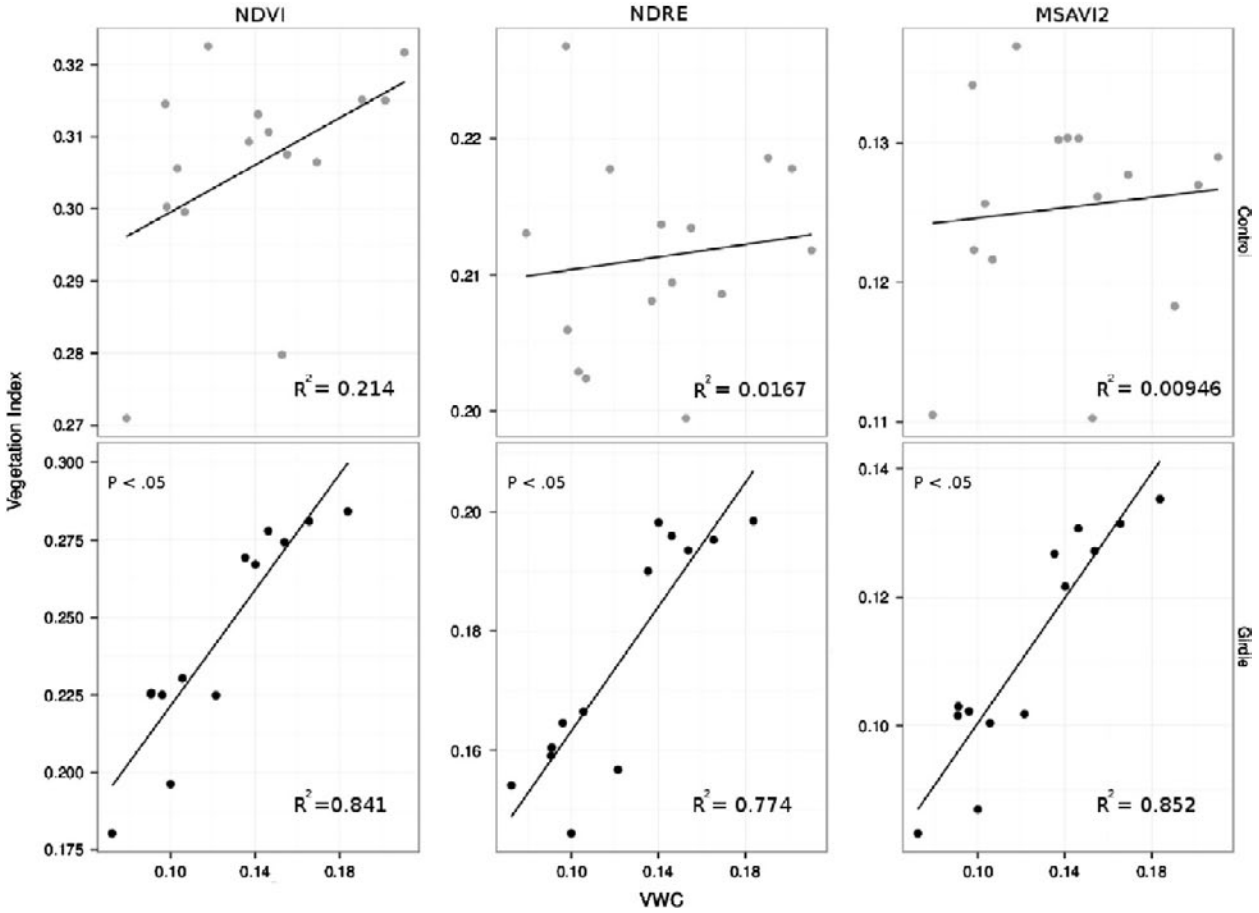

Fig. 7. Fetch-wide relationships between canopy vegetation indices and volumetric soil water at both the control (gray) and girdle (black) sites during periods where temperature and soil moisture are least limiting plant productivity (air temperature >0 °C and soil moisture >9%).

At the ecosystem scale, the high reduction in the system's capacity to take up CO_2 following the mortality of the large piñon was evident as a large reduction in GPP relative to the control site. After normalizing the fluxes between the control and girdled sites using pre-girdled fluxes at each site, it is clear that the piñon mortality triggered a cumulative loss of 540 g C m^{-2} taken up by the canopy through photosynthesis in the three years after the girdling (Fig. 3), resulting in a 25% decrease in productivity at the girdle site relative to control.

Landsat ETM+ and RapidEye were used to remotely sense the disturbance at girdled site (Fig. 4). The Landsat ETM+ NDVI (30 × 30 m pixels) begins to decline at the girdled site during the spring of 2010, following the winter snow melt, about 1 year following the disturbance. The canopy pixels monitored by RapidEye (5 × 5 m) show different trends and timing of green-up, with differences in NDVI 30 days following the girdling that persist throughout the time series (Fig. 4c).

The three RapidEye VI employed in this study showed rapid decreases in pixels dominated by girdled piñon by the end of 2009 (Fig. 4c). All three VI show the same downward trend due to the fact that there was a 25% loss of LAI at the onset of the manipulation. The RapidEye derived NDVI of the woody overstory decreased by approximately 40% by the end of 2011 (Fig. 4c). Following the first year of the disturbance, the girdled site continued to show decreases in VI at multiple scales, most likely due to the secondary mortality of small piñon.

3.2. Understory vegetation structural changes and ecosystem productivity

VI of the girdled crowns began to reverse their trajectories in 2011 from a downward to an upward trend (Fig. 5). This change in trajectory of the normalized VI suggests an increase in LAI of the pixels dominated by girdled vegetation, relative to the healthy overstory at the control site. Both NDVI and MSAVI2 mildly reflect this pattern; however, the NDRE shows a strong pattern of senescence and subsequent green-up, potentially indicating the growth of low LAI, high chlorophyll vegetation. The strong pattern exhibited by the NDRE to these changes might be explained by the high sensitivity of NDRE to both canopy structural properties and foliar biochemistry (e.g., Eitel et al., 2011; Gitelson & Merzlyak, 1996; Gitelson et al., 2005). Ground level analysis of the sites following the manipulation supports this observation and shows that the underlying cause of this green-up is the significantly ($P < 0.05$) higher establishment of annual forbs at the girdle site relative to the control site (Fig. 6). There were significant ($P < 0.05$) site effects in 2011 and 2012 but the interactions between canopy and interspace were not statistically significant. Furthermore, forb cover increased at the girdled site relative to control site, but we did not measure a statistically significant trend in the change in the relative cover of grasses or CAM functional types following the manipulation. The positive relationship between VWC and site averaged NDVI appeared to be influenced by this shift in understory structure as well, given the larger sensitivity on soil moisture to green-up at the girdled site ($R^2 = 0.21$ at the control site, $R^2 = 0.84$ at the girdle site) (Fig. 7). Both sites exhibit much weaker relationships between VWC and NDVI during drought conditions (Fig. 8).

The trends of the VI for interspace pixels suggest that the overstory manipulation altered the understory in open areas between the canopy cover in a very different way (Fig. 5). Over the course of each year the interspace vegetation at the girdle site decreased in both LAI and chlorophyll (as quantified by VI), suggesting the senescence of seasonal grasses and forbs. This is consistent with what we know of the function of these sites which capitalize on winter precipitation and monsoon precipitation, with a dry season in-between. However, the relative difference of the interspace vegetation for the girdle site compared to

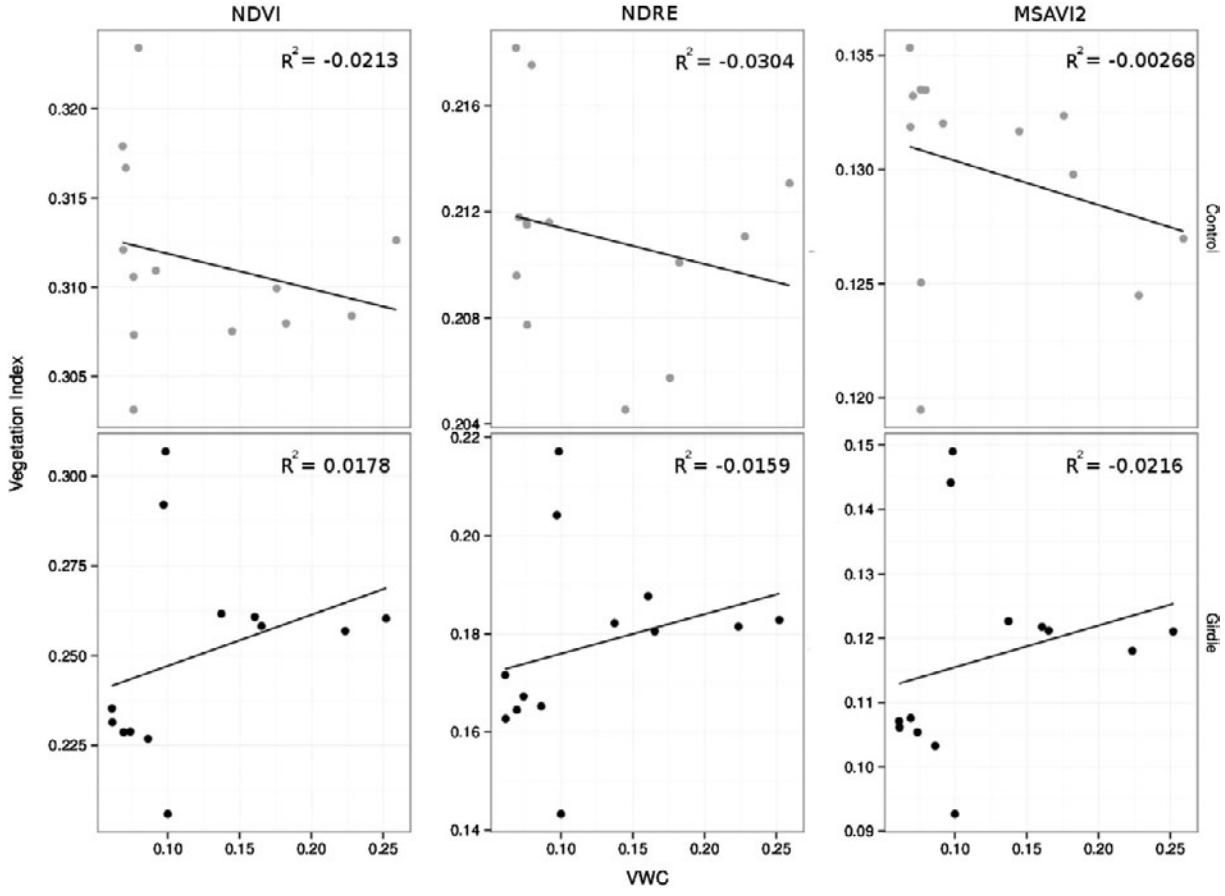

Fig. 8. Fetch-wide relationships between canopy vegetation indices and volumetric soil water at both the control (gray) and girdle (black) sites during periods where temperature and soil moisture are most limiting plant productivity (air temperature <0 °C or soil moisture <9%).

the control site indicates a differential senescence of the interspace vegetation at the girdle site (Fig. 5). This secondary effect suggests that the decrease in overstory vegetation has affected the longevity of the shallow rooting herbaceous vegetation in-between the canopy crowns. The year to year return to a consistent LAI and chlorophyll content of these interspace regions also indicates that this shift in the function of the interspace vegetation has not altered the initial winter moisture driven green-up that starts the herbaceous cycle each year, but rather has altered the ability of these plants to utilize monsoon precipitation.

3.3. Uncoupling of canopy reflectance and ecosystem function

Periods when soil water content is less limiting show a much stronger linear relationship between GPP and VI (Figs. 9 and 10) at the girdle site ($R^2 = 0.46$, $P < 0.05$) compared to the drought periods ($R^2 = 0.13$, $P > 0.05$). The control site also shows a decoupling between GPP and VI, but to a lesser degree ($R^2 = 0.22$, $P < 0.05$ during growing conditions, compared to $R^2 = 0.09$, $P > 0.05$ during drought conditions). Both of the sites are severely water limited, with the dominant control over GPP being soil moisture (Fig. 10). The rate at which the girdled site greens up with increases in soil water is now much greater relative to the control site (Figs. 7 and 8). The amount of green-up that occurs at the girdled site also has had a significant influence on the relationship between the VI and GPP, showing a greater initial slope relative to the control site. This suggests that the increase in understory vegetation has helped offset the uncoupled nature of the VI at the girdled site with GPP.

4. Discussion

4.1. Utility of time series imagery for canopy structural change detection

Our manipulation severely altered the structure of the ecosystem causing a variety of cascading effects on ecosystem function such as changes in phenology and the timing and magnitude of carbon uptake. This case study allowed us to characterize how well high spatial resolution (5 × 5 m) RapidEye imagery could be used to detect and characterize changes in canopy structure that followed as a result of the manipulation relative to coarser resolution Landsat ETM+ (30 × 30 m).

The initial mortality of the adult piñon at the girdle site resulted in a significant loss of leaf area, leaving the girdled fetch comprised of primarily juniper and non-reproductive piñon which is the normal species assemblage that typically survived following the severe regional drought and bark beetle outbreak of 1999–2002 (Clifford et al., 2008). Our girdling manipulation caused sudden drops in chlorophyll content just days following the disturbance (see Eitel et al., 2011) as opposed to weeks following the disturbance onset typically seen in taller, less arid coniferous canopies (Edburg et al., 2012). By the end of 2010, the girdled crowns were fully chlorotic (Fig. 2) and by the end of 2011 field allometric measurements suggested a loss of 33% of the leaf area at the girdled fetch.

The initial decline in foliar chlorophyll concentration seen before the end of 2009 was not reflected by Landsat ETM+ NDVI, most likely due to the coarser spatial resolution (30 × 30 m pixels) of the sensor being affected by the healthy juniper and small piñon crowns. The higher resolution RapidEye data (5 × 5 m) show a much faster response, with all

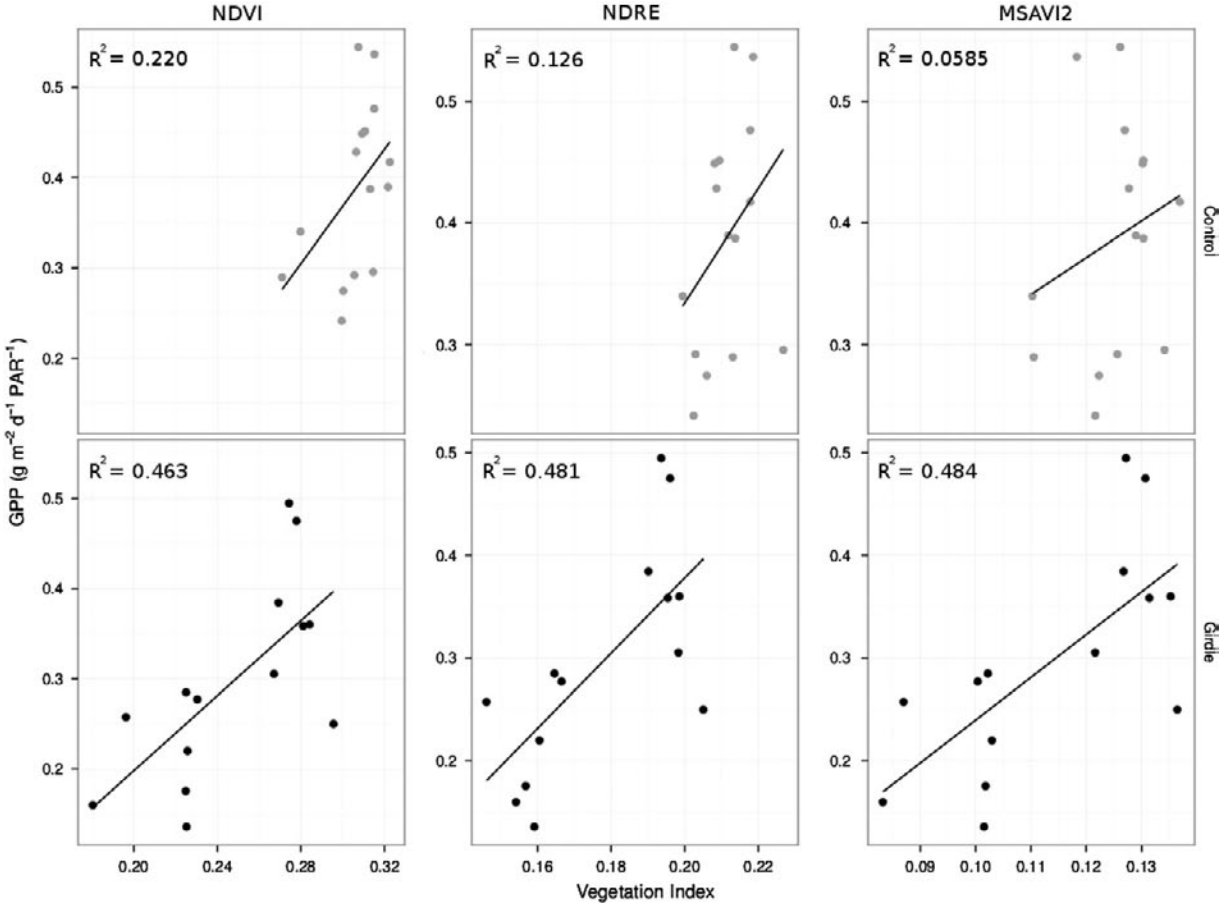

Fig. 9. Fetch-wide relationships between gross primary productivity and canopy vegetation indices at both the control (gray) and girdle (black) sites during periods where temperature and soil moisture are least limiting plant productivity (air temperature >0 °C or soil moisture <9%).

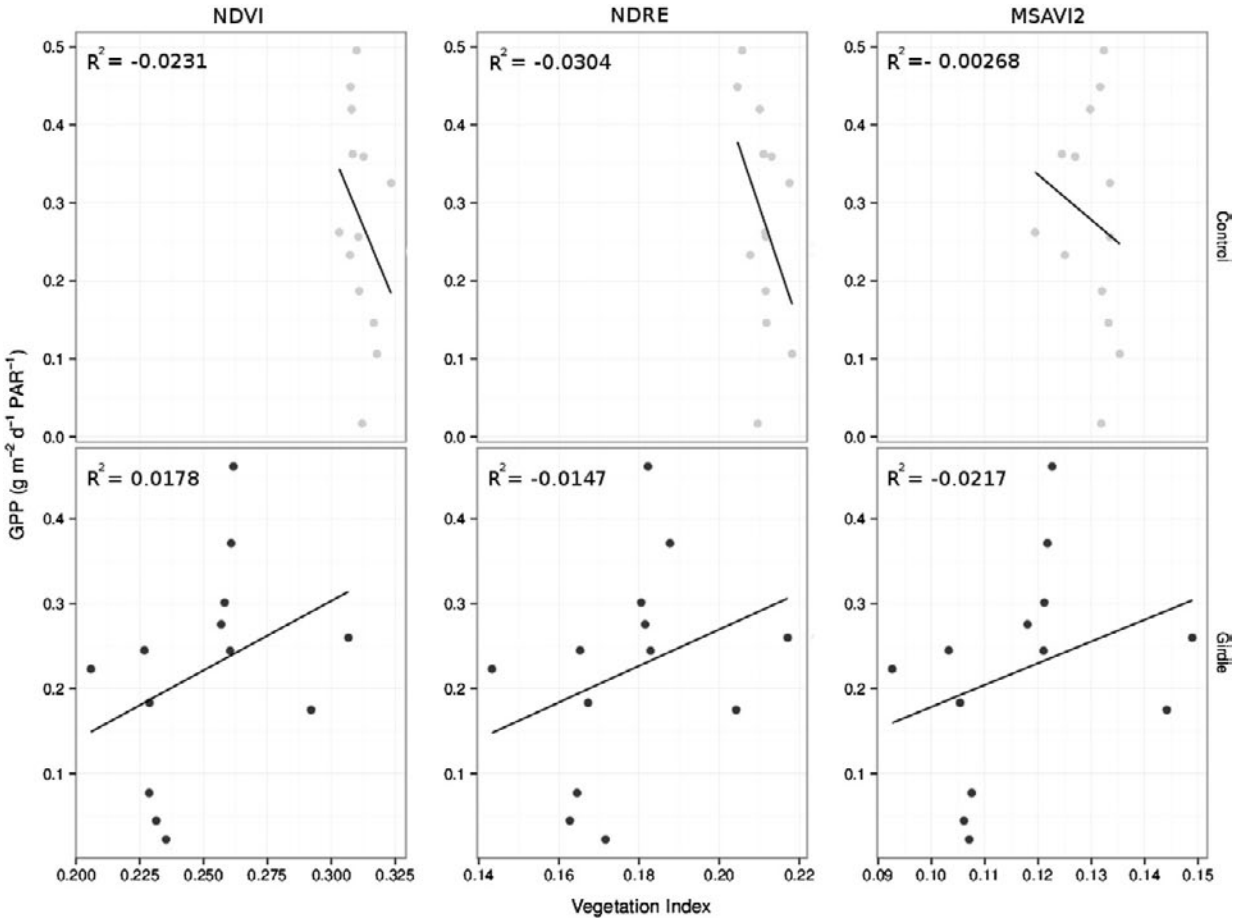

Fig. 10. Fetch-wide relationships between gross primary productivity and canopy vegetation indices at both the control (gray) and girdle (black) sites during periods where temperature and soil moisture are most limiting plant productivity (air temperature <0 °C or soil moisture <9%).

three VI reflecting the initial canopy stress. During this period, the RapidEye NDRE exhibited the highest sensitivity to the disturbance (see Eitel et al., 2011) and NDVI reflected the largest drop in canopy reflectance by the end of 2009. Landsat ETM + lagged in detecting the response relative to RapidEye by about 1 year. When the canopy became fully chlorotic in 2010, RapidEye and Landsat ETM + both detected large differences. In the final year of the experiment, the Landsat ETM + and RapidEye trends remain, as NDVI from both platforms continues to decline reflecting the mortality of the some of the remaining juniper or small piñon within the girdled tower fetch.

The first year that large structural changes begin to occur in the understory of the girdled piñon is 2011, as detected from RapidEye via NDVI and MSAVI2 (Fig. 5) when low LAI vegetation established under the girdled piñon crowns. This shift in understory structure, however, does not alter cumulative GPP at the girdle site, suggesting the establishment of forbs is not yet significant enough to alter GPP at the girdle site. In the long term, the increase in understory green-up may preclude the detection of the disturbance in the region, ultimately reducing the ability of remote sensing driven models of terrestrial carbon capture to accurately track post-mortality dynamics in these ecosystems (Huang et al., 2010). Our combined approach of structural analysis and in-situ carbon balance measurements may help circumvent these issues in the future, by allowing the structure-specific parameterization of remotely driven models of GPP.

The increase in herbaceous plants beneath the dead piñon trees at the girdle site may explain the large difference in the green-up response to soil moisture, relative to the control site. Figs. 7 and 8 highlight the uncoupled nature between the VI and soil water content at the control site (R^2 decreasing from 0.22 to 0.09 under low soil moisture conditions), contrasting with the stronger relationship at the girdle site (R^2 decreasing from 0.46 to 0.13 under low soil moisture conditions). The shallow rooting, herbaceous understory vegetation in this system was likely benefiting from increased needle deposition which can reduce nutrient, light and moisture competition (Breshears & Barnes, 1998) and facilitate leaf out.

4.2. Higher spatial resolution imagery aids semi-arid canopy change detection

Previous work in quantifying carbon stock losses in PJ woodlands (Huang, Asner, Martin, Barger, & Neef, 2009; Huang et al., 2012, 2010) has leveraged high resolution aerial imagery coupled with moderate resolution (30 m) satellite time series and spectral unmixing techniques to establish a relationship between the fraction of woody cover and biomass. The major advantage of this approach is the ability to scale estimates of NPP to the region and landscape. Within a single Landsat ETM + pixel, the spectral mixing approach can provide a fraction of woody to herbaceous cover, yet the specific relationship of where the herbaceous components are greening or senescing relative to the overstory cannot be ascertained. These spatially distributed relationships between overstory and understory structure are critical to understand in order to predict how disturbance will alter the function in semi-arid woodlands.

The 5 m spatial resolution of the RapidEye sensor and the temporal density of our time series allowed us to track individual clumps of crowns over time, and determine that the herbaceous establishment observed under the girdled piñon was not present between the girdled crowns. As a result, we can now establish a mechanistic understanding

of how this secondary understory structural changes are influencing ecosystem carbon balance, a yet uninvestigated topic which may have a significant impact at the regional and landscape scales. This cover specific response of the understory to overstory disturbance has been documented in other semi-arid regions and is consistent with the way these systems use light and water (Breshears & Barnes, 1998; Breshears & Rich, 1997; Rich et al., 2008), but to our knowledge has yet to be characterized remotely and understanding this effect on ecosystem scale changes in function is a requisite for the development of structure–function linked ecosystem models.

4.3. Monitoring the function of semi-arid biomes using satellite imagery hinges on water availability

Though the RapidEye derived indices performed well at tracking the structural changes in the ecosystem (reduction in canopy LAI, increase in the herbaceous green-up), the relationship between canopy reflectance and ecological function of the canopy was highly decoupled. Thus, linking remotely characterized changes in ecosystem structure with tower-measured GPP requires a more nuanced analysis, for example by using spectral information that has been shown to be sensitive to light use efficiency (Gamon et al., 1992; Gamon, Serrano, & Surfus, 1997). Given the semi-arid nature of PJ woodlands, as with all water limited systems, carbon uptake is generally governed by the presence of water (Fig. 11, Huxman et al., 2004; Muldavin, Moore, & Collins, 2008), which is stochastic and ephemeral. The uncoupling is essentially due to the fact that on most days, plant stomata have fully closed by late morning to resist desiccation, as vapor pressure deficit rises into the afternoon. Evergreen canopies typically respond to pulses of water by adjusting stomatal conductance and the rhizosphere, rather than up-regulating chlorophyll production or leaf area which is typically observed in herbaceous and deciduous vegetation (Huxman et al., 2004). Consequently, integrated measures of CO_2 uptake recorded by the tower show varying relationships with spectral VI such as NDRE, NDVI, and MSAVI2 that are sensitive to changes in chlorophyll content and LAI. By using our ground based measures of VWC, we can select only those days where soil water (and air temperature) were not limiting. This dramatically increases the strength of the linear relationship between the VI and GPP (Fig. 7), yet this relies on ground based estimates of soil water content. National soil moisture monitoring networks (e.g., the NRCS snowpack telemetry network) or the recent development of GPS based soil moisture monitoring (Larson et al., 2008) may potentially provide some of the required soil moisture data to parameterize future models of GPP in these sparse, semi-arid systems.

The dependence of the VI on soil moisture reflects the moisture limitations in these systems. Furthermore, this dependence suggests that the utility of the VI to monitor canopy status or predict GPP is contingent on there being sufficient moisture in the soil to allow photosynthesis to take place.

5. Conclusions

This case study focused on determining the potential role of satellite remote sensing in developing a more mechanistic understanding of the structural changes that take place in piñon juniper woodlands following disturbance events and how those structural changes affect the function of the ecosystem. We determined that both moderate (Landsat ETM+, 30 × 30 m pixel size) and high (RapidEye, 5 × 5 m pixel size) resolution satellite remote sensing platforms generally are capable of temporally resolving structural changes in piñon–juniper woodlands (PJ) following disturbance events. However, the complexity of the structure of PJ woodlands creates a highly heterogeneous mixture of live and dead vegetation, dense and sparse overstory, and the presence or absence of herbaceous constituents. This complex nature of PJ woodlands is what drives many researchers to leverage the spectral differences between those various ecosystem components by employing techniques such as spectral mixing analysis. This approach has worked well for determining the fraction of photosynthetic or non-photosynthetic woody vegetation, herbaceous cover, or bare soil in a moderately sized pixel (e.g., 30 × 30 m from Landsat TM or ETM+), yet the spatial relationship between the change in cover or function of these various constituents limits the ability to create a mechanistic understanding of the structural changes (e.g., how changes in the overstory relate to changes

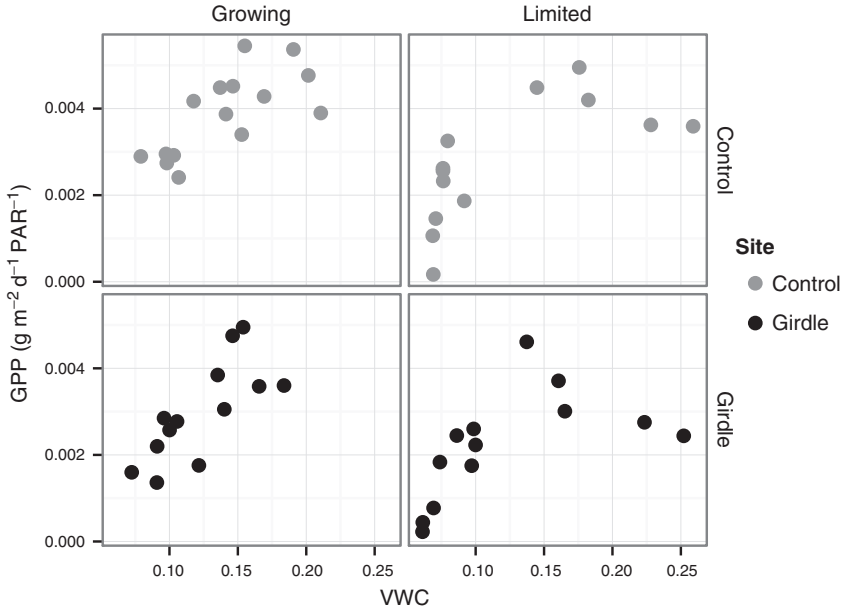

Fig. 11. Fetch-wide relationships between gross primary productivity and soil water content during growing (temperature >0 °C or soil moisture <9%) and growth limited (air temperature <0 °C or soil moisture <9%) conditions.

in the understory). To circumvent this challenge we utilized high spatial resolution data and determined that the structural response of the ecosystem following disturbance indeed has a spatial component. Specifically, the herbaceous ramp-up that occurred post-mortality was limited to the region below the crowns of dead trees. Further, the regions between the dead crowns showed almost the opposite result, suggesting the change in energy balance of the ecosystem following the loss of the canopy reduced the ability of the herbaceous layer to establish in crown interspaces after the disturbance.

The impact of these structural changes on the function of the ecosystem was difficult to remotely determine. Initially, the loss of canopy following the disturbance was readily tracked by remote sensing platforms at multiple spatial scales, with high spatial resolution data (5×5 m) allowing detection almost a full year earlier. However, relating remote sensing data of the disturbance event and the subsequent recovery of the herbaceous layer with the in-situ measures of ecosystem productivity measured by flux towers yielded poor relationships. Our data suggest that this phenomenon is due to the uncoupling of the reflectance of the ecosystem with the function of the ecosystem during periods of drought, which for PJ woodlands can represent a large portion of the year. Consequently, we conclude that the inclusion of high spatial resolution satellite time series can aid in developing mechanistic models of recovery from disturbance in these heterogeneous systems, but future work should focus on ways to improve our ability to predict canopy function even during periods of drought which pervade this widespread and sensitive southwestern biome.

Acknowledgments

This research was supported primarily by the Office of Science (BER), US Department of Energy. We also acknowledge the funding from grant/cooperative agreement number 08HQGR0157 from the United States Geological Survey (USGS) via a subaward from AmericaView, the National Science Foundation through funds to the Sevilleta LTER site and NM EPSCoR, in addition to the funding from the USFS for support of the flux towers, and from the New Mexico Space Grant Consortium (NMSGC) for the partial funding of satellite data acquisitions. Its contents are solely the responsibility of the authors and do not necessarily represent the official views of the Office of Science, US Department of Energy, NSF, or USGS. Many thanks to Andy Fox, Leo Stoscheck and Skyler Hackley for the intellectual and physical support of this project, and to Nate McDowell, Thom Rahn and Bob Sinsabaugh for their help in establishing the treatments. We also thank RapidEye for making a portion of the dense time series freely available for this study. Finally we thank the three anonymous reviewers and David Turner for their comments and revisions that greatly improved the quality of the manuscript.

References

Adams, H., Macalady, A., Breshears, D. D., Allen, C. D., Stephenson, N. L., Saleska, S. R., Huxman, T. E., & McDowell, N. (2010). Climate- Induced Tree Mortality: Earth System Consequences. *Eos, Transactions*, *91*, 2009–2011.

Allen, C. D., Macalady, A. K., Chenchouni, H., Bachelet, D., Mcdowell, N., Vennetier, M., et al. (2010). A global overview of drought and heat-induced tree mortality reveals emerging climate change risks for forests. *Forest Ecology and Management*, *660–684*.

Anderson-Teixeira, K. J., Delong, J. P., Fox, A.M., Brese, D. A., & Litvak, M. E. (2011). Differential responses of production and respiration to temperature and moisture drive the carbon balance across a climatic gradient in New Mexico. *Global Change Biology*, *17*, 410–424.

Asner, G. P., & Heidebrecht, K. B. (2002). Spectral unmixing of vegetation, soil and dry carbon cover in arid regions: Comparing multispectral and hyperspectral observations. *International Journal of Remote Sensing*, *23*, 3939–3958.

Breshears, D.D., & Barnes, F. J. (1998). Interrelationships between plant functional types and soil moisture heterogeneity for semiarid landscapes within the grassland/forest continuum: A unified conceptual model. *Landscape Ecology*, *14*, 465–478.

Breshears, D.D., Cobb, N. S., Rich, P.M., Price, K. P., Allen, C. D., Balice, R. G., et al. (2005). Regional vegetation die-off in response to global-change-type drought. *Proceedings of the National Academy of Sciences of the United States of America*, *102*, 15144–15148.

Breshears, D., & Rich, P. (1997). Overstory-imposed heterogeneity in solar radiation and soil moisture in a semiarid woodland. *Ecological Applications*, *4*, 1201–1215.

Chavez, P. S. (1988). An improved dark-object subtraction techniquefor atmospheric scattering correction of multispectral data. *Remote Sensing of Environment*, *24*, 459–479.

Canty, M., & Nielsen, A. (2008). Automatic radiometric normalization of multitemporal satellite imagery with the iteratively re-weighted MAD transformation. *Remote Sensing of Environment*, *112*, 1025–1036.

Chen, X., Vierling, L. A., Rowell, E., & DeFelice, T. (2004). Using lidar and effective LAI data to evaluate IKONOS and Landsat 7 ETM+ vegetation cover estimates in a ponderosa pine forest. *Remote Sensing of Environment*, *91*(1), 14–26.

Choat, B., Jansen, S., Brodribb, T. J., Cochard, H., Delzon, S., Bhaskar, R., Bucci, S. J., Feild, T. S., Gleason, S. M., Hacke, U. G., Jacobsen, A. L., Lens, F., Maherali, H., Martínez-Vilalta, J., Mayr, S., Mencuccini, M., Mitchell, P. J., Nardini, A., Pittermann, J., Pratt, R. B., Sperry, J. S., Westoby, M., Wright, I. J., & Zanne, A. E. (2012). Global convergence in the vulnerability of forests to drought. *Nature*, *491*, 752–755.

Clifford, M., Rocca, M., & Delph, R. (2008). Drought induced tree mortality and ensuing Bark beetle outbreaks in Southwestern pinyon–juniper woodlands. *USDA Forest Service Proceedings* (pp. 39–51).

Coops, N. C., Johnson, M., Wulder, M. A., & White, J. C. (2006). Assessment of Quickbird high spatial resolution imagery to detect red attack damage due to mountain pine beetle infestation. *Remote Sensing of Environment*, *103*, 67–80.

Collett, L. J., Goulevitch, B. M., & Danaher, T. J. (1997). SLATSRadiometric Correction: A Semi-automated, Multi-stage Processfor the Standardisation of Temporal and Spatial Radiometric Differences. *Queensland Department of Natural Resources* URL:http://www.nrm.qld.gov.au/slats/pdf/arspc9_rad_corrections1.pdf

Detto, M., Montaldo, N., Albertson, J.D., Mancini, M., & Katul, G. (2006). Soil moisture and vegetation controls on evapotranspiration in a heterogeneous Mediterranean ecosystem on Sardinia, Italy. *Water Resources Research*, *42*, 1–16.

Edburg, S. L., Hicke, J. A., Brooks, P. D., Pendall, E. G., Ewers, B. E., Norton, U., et al. (2012). Cascading impacts of bark beetle-caused tree mortality on coupled biogeophysical and biogeochemical processes. *Frontiers in Ecology and the Environment*, *10*, 416–424.

Eitel, J. U. H., Long, D. S., Gessler, P. E., Hunt, E. R., & Brown, D. J. (2009). Sensitivity of ground-based remote sensing estimates of wheat chlorophyll content to variation in soil reflectance. *Soil Science Society of America Journal*, *73*, 1715.

Eitel, J. U. H., Vierling, L. A., Litvak, M. E., Long, D. S., Schulthess, U., Ager, A. A., et al. (2011). Broadband, red-edge information from satellites improves early stress detection in a New Mexico conifer woodland. *Remote Sensing of Environment*, *115*, 3640–3646.

Elmore, A. J., Mustard, J. F., Manning, S. J., & Lobell, D. B. (2000). *Quantifying Vegetation Change in Semiarid Environments : Precision and Accuracy of Spectral Mixture Analysis and the Normalized Difference Vegetation Index*, *102*, 87–102.

Flanagan, L., Wever, L., & Carlson, P. (2002). Seasonal and interannual variation in carbon dioxide exchange and carbon balance in a northern temperate grassland. *Global Change Biology*, *8*, 599–615.

Fox, A. J., Hilton, T., Krofcheck, D. J., Sinsabaugh, R. L., Pendleton, R., Dettweiler-Robinson, E., et al. (2013). Ecosystem experimental manipulation and model-data fusion to quantify carbon cycle dynamics to piñon pine mortality. *Global Change Biology*.

Gamon, J. A., Penuelas, J., & Field, C. B. (1992). A narrow-waveband spectral index that tracks diurnal changes in photosynthetic efficiency. *Remote Sensing of Environment*, *41*, 35–44.

Gamon, J., Serrano, L., & Surfus, J. (1997). The photochemical reflectance index: An optical indicator of photosynthetic radiation use efficiency across species, functional types, and nutrient levels. *Oecologia*, *112*, 492–501.

Gitelson, A., & Merzlyak, M. (1996). Signature analysis of leaf reflectance spectra: Algorithm development for remote sensing of chlorophyll. *Journal of Plant Physiology*, *148*, 494–500.

Gitelson, A., Vina, A., Ciganda, V., & Rundquist, D. C. (2005). Remote estimation of canopy chlorophyll content in crops. *Geophysical Research Letters*, *32*, 4–7.

Hsieh, C., Katul, G., & Chi, T. (2000). An approximate analytical model for footprint estimation of scalar fluxes in thermally stratified atmospheric flows. *Advances in Water Resources*, *23*, 765–772.

Huang, C., Asner, G., & Barger, N. (2012). Modeling regional variation in net primary production of pinyon–juniper ecosystems. *Ecological Modelling*, *227*, 82–92.

Huang, C., Asner, G. P., Barger, N. N., Neff, J. C., & Floyd, M. L. (2010). Regional aboveground live carbon losses due to drought-induced tree dieback in piñon–juniper ecosystems. *Remote Sensing of Environment*, *114*, 1471–1479.

Huang, C., Asner, G., Martin, R., Barger, N. N., & Neef, J. C. (2009). Multiscale analysis of tree cover and aboveground carbon stocks in pinyon–juniper woodlands. *Ecological Applications*, *19*, 668–681.

Huete, A. R., Jackson, R. D., & Post, D. F. (1985). Spectral response of a plant canopy with different soil backgrounds. *Remote Sensing of Environment.*, *17*, 37–53.

Huete, A. R. (1988). A soil-adjusted vegetation index (SAVI). *Remote Sensing of Environment*, *25*, 53–70.

Huete, A. R. (1989). Soil influences in remotely sensed vegetation-canopy spectra. In G. Asrar (Ed.), *Theory and Applications of Optical Remote Sensing* (pp. 107–141).

Huxman, T. E., Snyder, K. A., Tissue, D., Leffler, A. J., Ogle, K., Pockman, W. T., et al. (2004). Precipitation pulses and carbon fluxes in semiarid and arid ecosystems. *Oecologia*, *141*, 254–268.

IPCC (2007). *Climate Change 2007: The Physical Science Basis*. Contribution of Working Group I to the Fourth Assessment Report of the Intergovernmental Panel on Climate Change. UK and New York: Cambridge University Press, Cambridge.

Jenkins, J. C., Chojnacky, D. C., Heath, L. S., & Birdsey, R. A. (2003). National-scale biomass estimators for United States tree species. *Forest Science*, *49*, 12–35.

Kennedy, R., Cohen, W., & Schroeder, T. (2007). Trajectory-based change detection for automated characterization of forest disturbance dynamics. *Remote Sensing of Environment*, *110*, 370–386.

Kennedy, R. E., Yang, Z., & Cohen, W. B. (2010). Remote Sensing of Environment Detecting trends in forest disturbance and recovery using yearly Landsat time series: 1. LandTrendr: Temporal segmentation algorithms. *Remote Sensing of Environment*, *114*, 2897–2910.

Larson, K. M., Small, E. E., Gutmann, E. D., Bilich, A. L., Braun, J. J., & Zavorotny, V. U. (2008). Use of GPS receivers as a soil moisture network for water cycle studies. *Geophysical Research Letters*, *35*, 24.

Lasslop, G., Reichstein, M., Papale, D., Richardson, A.D., Arneth, A., Barr, A., et al. (2010). Separation of net ecosystem exchange into assimilation and respiration using a light response curve approach: Critical issues and global evaluation. *Global Change Biology*, *16*, 187–208.

Li, X., Gao, Z., Bai, L., & Huang, Y. (2012). Potential of high resolution RapidEye data for sparse vegetation fraction mapping in arid regions. *Geoscience and Remote Sensing Symposium (IGARSS). 2012 IEEE International.* (pp. 420–423).

Liu, S., Bond-Lamberty, B., & Hicke, J. (2011). Simulating the impacts of disturbances on forest carbon cycling in North America: Processes, data, models, and challenges. *Journal of Geophysical Research*, *116*, 1–22.

Massman, W. (2000). A simple method for estimating frequency response corrections for eddy covariance systems. *Agricultural and Forest Meteorology*, *104*, 185–198.

Muldavin, E., Moore, D., & Collins, S. (2008). Aboveground net primary production dynamics in a northern Chihuahuan Desert ecosystem. *Oecologia*, *155*, 123–132.

Nielsen, A., Conradsen, K., & Simpson, J. (1998). Multivariate alteration detection (MAD) and MAF postprocessing in multispectral, bitemporal image data: New approaches to change detection studies. *Remote Sensing of Environment*, *64*, 1–19.

Qi, J., Chehbouni, A., & Huete, A. (1994). A modified soil adjusted vegetation index. *Remote Sensing of Environment*, *48*, 119–126.

R Core Team (2013). R: A language and environment for statistical computing. Vienna, Austria. http://www.R-project.org

Rich, P.M., Breshears, D.D., & White, A.B. (2008). Phenology of mixed woody–herbaceous ecosystems following extreme events: Net and differential responses. *Ecological Society of America*, *89*, 342–352.

Royer, P. D., Cobb, N. S., Clifford, M. J., Huang, C. -Y., Breshears, D.D., Adams, H. D., et al. (2011). Extreme climatic event-triggered overstorey vegetation loss increases understorey solar input regionally: Primary and secondary ecological implications. *Journal of Ecology*, *99*, 714–723.

Schwalm, C. R., Williams, C. A., Schaefer, K., Baldocchi, D., Black, T. A., Goldstein, A. H., et al. (2012). Reduction in carbon uptake during turn of the century drought in western North America. *Nature Geoscience*, *5*, 551–556.

Shaw, J., Steed, B., & DeBlander, L. (2005). Forest Inventory and Analysis (FIA) annual inventory answers the question: What is happening to pinyon–juniper woodlands? *Journal of Forestry*, *103*, 280–285.

Spruce, J., Sader, S., Ryan, R., & Smoot, J. (2010). Assessment of MODIS NDVI time series data products for detecting forest defoliation by gypsy moth outbreaks. *Remote Sensing of Environment*, *115*, 427–437.

Storey, T. O. (2004). *Estimating sagebrush cover in a portion of the Pinedale Anticline Project.* University of Wyoming, Department of Geography.

Tong, A., & He, Y. (2013). Comparative analysis of SPOT, Landsat, MODIS, and AVHRR normalized difference vegetation index data on the estimation of leaf area index in a mixed grassland ecosystem. *Journal of Applied Remote Sensing*, *7*, 073599.

Tucker, C. (1979). Red and photographic infrared linear combinations for monitoring vegetation. *Remote Sensing of Environment*, *8*, 127–150.

Wang, Q., Adiku, S., Tenhunen, J., & Granier, A. (2005). On the relationship of NDVI with leaf area index in a deciduous forest site. *Remote Sensing of Environment*, *94*, 244–255.

Webb, E., Pearman, G. I., & Leuning, R. (1980). Correction of flux measurements for density effects due to heat and water vapour transfer. *Quarterly Journal of the Royal Meteorological Society*, *106*, 85–100.

Williams, A., Allen, C., & Macalady, A. (2012). Temperature as a potent driver of regional forest drought stress and tree mortality. *Nature Climate*, *3*, 8–13.

Yang, J., Weisberg, P. J., & Bristow, N. A. (2012). Landsat remote sensing approaches for monitoring long-term tree cover dynamics in semi-arid woodlands: Comparison of vegetation indices and spectral mixture analysis. *Remote Sensing of Environment*, *119*, 62–71.

Williams, A., Allen, C., Millar, C. I., Swetnam, T. W., Michaelsen, J., Still, C. J., et al. (2010). Forest responses to increasing aridity and warmth in the southwestern United States. *Proceedings of the National Academy of Sciences*, *107*, 21289–21294.

Wulder, M. A., Dymond, C. C., White, J. C., Leckie, D. G., & Carroll, A. L. (2006). Surveying mountain pine beetle damage of forests: A review of remote sensing opportunities. *Forest Ecology and Management*, *221*, 27–41.